Radiotherapy and Oncology 138 (2019) 17–24

Contents lists available at ScienceDirect

Radiotherapy and Oncology

journal homepage: www.thegreenjournal.com

Original Article

Micro cone beam computed tomography for sensitive assessment of radiation-induced late lung toxicity in preclinical models

D. van Berlo [a], A. Khmelinskii [b,1], A. Gasparini [b,1], F.J. Salguero [b], B. Floot [a], N. de Wit [c], M. van de Ven [c], J.Y. Song [d], R.P. Coppes [e], M. Verheij [a,b], J.J. Sonke [b], C. Vens [a,b,*]

[a] Division of Cell Biology; [b] Department of Radiation Oncology; [c] Mouse Clinic for Cancer and Aging (MCCA) Preclinical Intervention Unit; [d] Department of Experimental Animal Pathology, The Netherlands Cancer Institute, Amsterdam; and [e] Department of Radiation Oncology and Department of Biomedical Sciences of Cells & Systems, Section Molecular Cell Biology, University Medical Center Groningen, The Netherlands

ARTICLE INFO

Article history:
Received 26 October 2018
Received in revised form 2 May 2019
Accepted 3 May 2019
Available online 27 May 2019

Keywords:
Preclinical lung models
Lung fibrosis
μIGRT
Normal tissue toxicity
μCBCT

ABSTRACT

Background and purpose: Preclinical models are much needed to assess the effect of novel radiosensitizers or mitigators on radiation dose limiting lung toxicity. Albeit showing radiation-induced lung pathologies, current mouse models lack the sensitivity to do so. Using micro image-guided radiotherapy (μIGRT) techniques, we aimed to establish murine models which enable the sensitive detection of lung damage aggravation and characterized functional, radiological and histological responses.

Materials and methods: Right lungs of C57Bl/6J mice were irradiated using μIGRT with doses from 15 to 27 Gy and with 21 Gy and cisplatin as a radio-sensitizer in a second study. Mice were sacrificed for histological and pathological assessment at different time-points post-IR. Lung density was determined using the integrated micro cone-beam CT (μCBCT). Lung function was measured by double-chamber-plethysmography.

Results: μIGRT resulted in accurate deposition of the radiation dose in the right lung only as determined by γH2AX staining. Lung fibrosis was confirmed by pathological assessments and increased significantly at 21 Gy as determined by automated quantification of histochemical analyses. Lung function was affected in a dose-dependent manner. μCBCT-determined lung densities increased significantly over time in the irradiated lungs and showed a strong radiation dose-dependence. Importantly, the μCBCT analyses allowed the detection of additional lung damage caused by 3 Gy dose increments or by the combination with cisplatin.

Conclusion: μCBCT after right lung μIGRT enables the sensitive detection of effects inflicted by relative small dose increments or radio-sensitizers. Our preclinical model therefore facilitates the determination of lung damage exacerbation for the safety assessment of novel RT-drug combinations.

Radiotherapy is a mainstay in lung cancer treatment, however overall survival still remains poor [1]. Novel treatments for lung cancer are urgently needed and several strategies are currently under investigation. Some promising approaches aim to sensitize tumor cells to radiotherapy by administering molecular targeted agents. To evaluate the potential adverse effects of such new therapies in healthy tissues, preclinical models should be (1) sensitive, (2) robust and (3) clinically relevant by applying modern technologies. By meeting these criteria they could provide better guidance for Phase I clinical trials in which novel radiotherapy regimens are tested.

Symptomatic pneumonitis and pulmonary fibrosis are dose-limiting clinical toxicities associated with radiotherapy in the thoracic region. Murine pulmonary fibrosis models to address radiation induced lung toxicities have been successfully established in the past by using radiation lung fibrosis prone C57Bl6/J mice [2,3]. Due to the lack of technological advances in small animal radiation techniques, past pre-clinical models and data were, however, limited by the applied large volumes, usually involving the whole thorax or half of it (hemi-thoracic irradiation). In these models, and different from the clinical setting, co-irradiation of the bone marrow and the heart might have influenced the lung toxicity endpoints under investigation. Data from van Luijk et al. [4,5] show that co-irradiation of the heart impacts on radiation induced lung toxicity in rats and can induce pleural effusion [6]. Such heart–lung links have also been observed in patients [7]. This further highlights the potential complex interaction of tissues in radiation-

* Corresponding author at: Division of Cell Biology and Department of Radiation Oncology, The Netherlands Cancer Institute, Plesmanlaan 122, 1066 CX Amsterdam, The Netherlands.
E-mail address: c.vens@nki.nl (C. Vens).
[1] These authors contributed equally.

https://doi.org/10.1016/j.radonc.2019.05.007
0167-8140/

induced toxicities and the importance of clinically relevant radiation practices in pre-clinical models. Micro-Image-Guided Radiotherapy (μIGRT) for small animals provides accurate irradiation and image guidance by cone beam computed tomography (μCBCT) [8–10]. The integrated μCBCT can also be used to assess lung density for the assessment of radiation-induced pulmonary pathologies [11].

In the current work, we aim to establish a pre-clinical late lung toxicity model by applying advanced preclinical μIGRT and μCBCT technologies that allow the accurate irradiation of one lung, while sparing other tissue such as the heart. Here we report feasibility and accuracy of the model and describe the dose–response relationships of late fibrotic responses after such treatment and their impact on lung function. As these models are intended to guide clinical practice for novel RT/drug combinations, we tested the ability to identify dose response changes using different histological and clinically relevant lung toxicity endpoints in a longitudinal study design. Next, we evaluated the potential of such a preclinical radiation-induced lung toxicity model in detecting lung damage aggravation by the combination with the radio-sensitizer cisplatin.

Materials and methods

Mice

Male C57Bl6/J mice were obtained from Charles River (L'Arbresle, France). Housing and all animal experimental procedures were performed according to national and European ethical regulations and were approved by the institute's Animal Ethical Committee.

Irradiation

Ten week old mice at a mean weight of 22.9 g (+/−1.2) were irradiated under full anesthesia (2.5% isoflurane inhalation) with single doses on the right lung (RL) using the X-RAD 225Cx μIGRT system at 225 kV, 13 mA (Precision X-ray Inc., North Branton, US). A single beam shaped by a custom-made collimator to spare critical organs was pointed perpendicular to the mouse in prone position (Fig. 1A, Sup-Fig. S1). Control mice were sham-irradiated. 10 mice were assigned to each group. Mice in the first dose response study were treated and housed in the old NKI animal facility. The integrated μCBCT was used for accurate radiation beam positioning. We used the SmART Planning system (MAASTRO Clinic, Maastricht, NL, [12]) to simulate the dose distribution of the treatment and to derive a representative DVH. The effect of positioning errors (up to 0.3 mm) was simulated. Mice were irradiated after automatic registration on the RL using the reference image derived from a pilot study to generate the collimator. Mice were sacrificed after 1 h for target evaluation by γH2AX histochemistry or followed for 40 weeks until euthanasia by i.p. injections pentobarbital.

Histology and (immuno) histochemistry

Lungs were fixated by intra-tracheal infusion with EAF fixative (ethanol/acetic acid/formaldehyde/saline at 40:5:10:45 v/v/v/v). After 24 h EAF-fixation, tissues were embedded in paraffin and sectioned for histology. Hematoxylin-Eosin-Saffrane, Sirius red and Masson's trichrome staining was performed according to standard protocols. Anti-γH2AX (Cell Signaling) was used for γH2AX

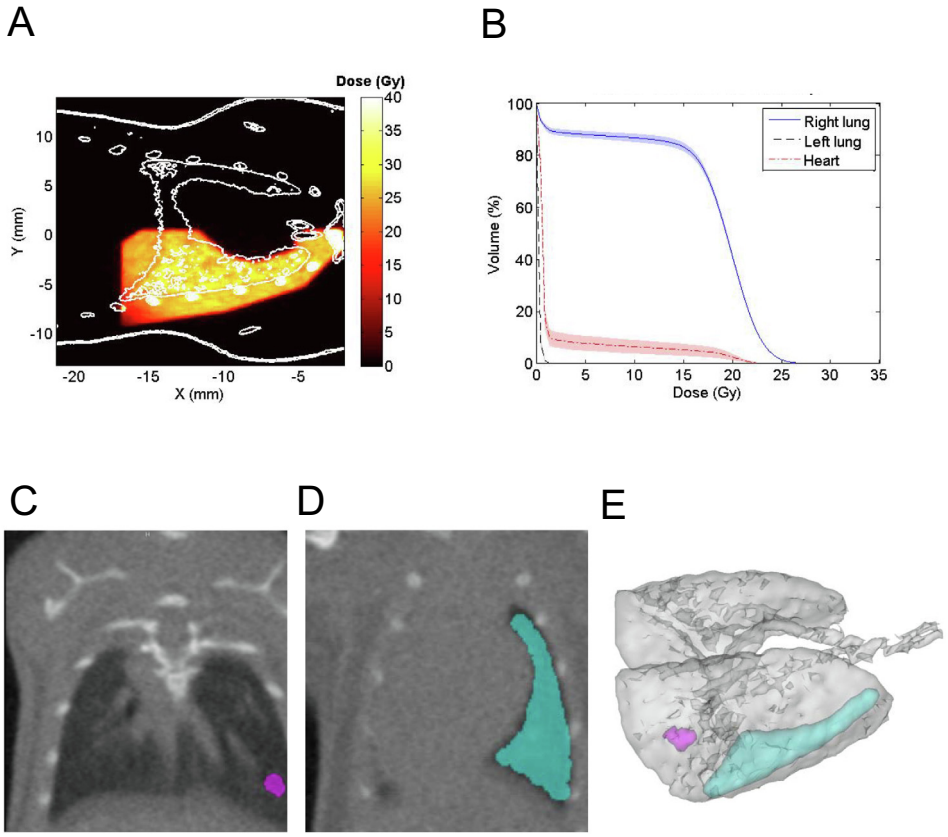

Fig. 1. (A) Representative image of the radiation field for a 27 Gy-exposed mouse. (B) Dose-volume histogram (DVH) of a 27 Gy-exposed mouse. (C–E) Visual representation of sub-volumes used in the fully automated (C) and 2.5D (D) right lung density quantifications and locations of those regions within the right lung depicted in 3D (E).

immuno-histochemistry. For quantification, images of whole lung tissue sections were made using an Aperio Scanscope AT2 (Leica Biosystems) at 20× magnification. Annotation fields were drawn as shown in Sup-Fig. 2A while avoiding large airways or blood vessels (Sup-Fig. 2B). "Staining concentration" values were determined using the "Measure Stained Area" algorithm (Sup-Fig. 2C) provided in the SlidePath Version 4.0.6 (Leica MicroSystems, Dublin, Ireland).

Lung function measurement

Breathing rates were measured using a mouse double-chamber plethysmograph (model PLY210, EMMS, Hampshire, UK) forty weeks post-irradiation. Data were gathered during a period of 20 min after a 20 min acclimation time. Breathing rates were quantified using the eDaqc version 1.7 software package (EMMS, Bordon, UK).

μCBCT lung density quantification

μCBCT scans (voxel size $0.1 \times 0.1 \times 0.1$ mm^3) were acquired at 100 kV to quantify lung densities in the different radiation dose groups 8, 34, 37 and 40 weeks post-irradiation. Fully automated registration and propagation of sub-volumes of the lungs provided the μCBCT density values. These were compared and validated to lung density values derived from a manual selection of a specific coronal plane slice (termed 2.5D method; Fig. 1C–E). Density quantification methods are described in detail in Sup-Methods.

Cisplatin radiation combination study

A second independent study was conducted in the new Mouse Clinic for Cancer and Ageing (MCCA) at the NKI to assess the impact of drug radiation combinations. Ten to eleven week old male C57Bl6/J mice were irradiated under full anesthesia (2.5% isoflurane inhalation) with single doses on the right lung (RL) using the X-RAD 225Cx μIGRT system, followed by regular (monthly) μCBCT scans as described above. Each treatment group contained ten mice at the start of the study. Two groups received cisplatin (3 mg/kg b.w.) on three consecutive days prior to irradiation (CIS-21Gy) or sham-radiation (CIS−0Gy). Control groups consisted of 21 Gy irradiated mice with or without *i.p.* injections of the vehicle solution and the corresponding sham (0 Gy) treated groups. Data are shown until 36 weeks post-irradiation, however not all mice reached the end of the study due to treatment unrelated causes. Statistical analyses were therefore conducted on the data until 21 weeks to assure the assessment of at least 8 mice per group and appropriate AUC comparisons.

Statistical analysis

One-way ANOVA with Dunnett's post-hoc test was performed for group comparisons using SPSS or GraphPad Prism software. A repeated *t*-test with Holm-Sidak correction for multiple testing was applied to test for differences between the right and left lung staining data. When assessing AUC (area under the curve), individual mouse radiodensity values were normalized to the corresponding week 0 value of that mouse. Individual AUC values were generated from these radiodensity data (in post-irradiation days for accuracy) from week 0 to 21 using GraphPad Prism software. Groups were then compared using ANOVA with Holm-Sidak correction for multiple testing.

Results

Feasibility and accuracy of mouse lung μIGRT

Here we set out to establish a preclinical mouse lung fibrosis model which applies large radiation fields that however exclude the heart and other critical organs. For this purpose, we used C57Bl6/J mice which are fibrosis-prone and develop radiation-induced fibrosis within 20 weeks (depending on dose and volumes) [6,13–17]. The intention was to establish a preclinical model able to sensitively detect potential toxicity changes by novel combined treatments (*i.e.* addition of drugs). Therefore we chose large volumes and single fractions regimens. A custom-made collimator for single field radiation of the right lung was therefore constructed based on μCBCT analyses of five mice at the intended study age (Sup-Fig. S1A–D). Mice in prone position were irradiated from the top with a single vertical beam for maximum coverage of the right lung while sparing most of the heart. The radiated lung volumes averaged to approximately 0.3 cm^3. Fig. 1 shows the radiation fields and the projection on the tissue outlines demonstrates inclusion of the right lung and exclusion of the heart in these mice. The DVHs confirm that more than 90% of the heart is spared from high dose (<10% of administered dose) exposure and show a minimal involvement of the left lung (Fig. 1B).

γH2AX immunohistochemistry confirmed targeted radiation of the right lung (Fig. 2A and B). The heart was largely excluded from damage (Sup-Fig. S3A-B). γH2AX staining intensities did not exceed those caused by intentional control irradiations to the heart with 1 Gy (Sup-Fig. S3B). Whole lung mean γH2AX values in the left lungs are low and confirm effective shielding of the left lung. Mean left lung values are slightly increased compared to sham-treated (Fig. 2A); a result caused by the overlap of the right and left lung lobes in the basal region. We conclude that μIGRT of the right lung, while sparing the heart to a large extent, is feasible.

Dose-dependent development of lung fibrosis pathology

We next assessed the development of lung fibrosis and in particular the dose dependence of this process in this model. Mice received single radiation doses ranging from 15 to 27 Gy and were followed for 40 weeks before being sacrificed for histopathological assessments. Lung fibrosis was confirmed by the animal pathologist in the high radiation dose levels groups. The right lung showed increased amount of collagen staining in the peri-vascular/bronchiolar spaces and alveolar septa (Fig. 3B). To assess the extent of fibrosis quantitatively, we determined collagen deposition by two independent staining protocols, Masson's trichrome and Sirius red (Fig. 3, Sup-Fig. S2). Fig. 3 depicts the average Sirius red staining concentration values from the lungs in the different animal groups. Right lung staining concentration values were significantly increased in mice irradiated with 21 Gy or more. No significant alterations were found in the left lung, further confirming targeting and excluding other possible systemic influences. Masson's trichrome staining confirmed this pattern (Sup-Fig. S4). Notably, the sigmoid-like shape of the figure suggests a threshold damage or saturation feature. When assessing collagen deposition in alveolar compartments within the lung we found a similar pattern across the different areas of the lung (Sup-Fig. S5). These histological data confirm the development of fibrosis in these mice and our data indicate a threshold dose of 21 Gy for pronounced (histochemically confirmed) lung fibrosis in mice at 40 weeks after unilateral lung irradiation without heart involvement.

Induction of lung function impairment

Lung function deterioration caused by radiation-induced pulmonary fibrosis is a critical and relevant endpoint in the clinic.

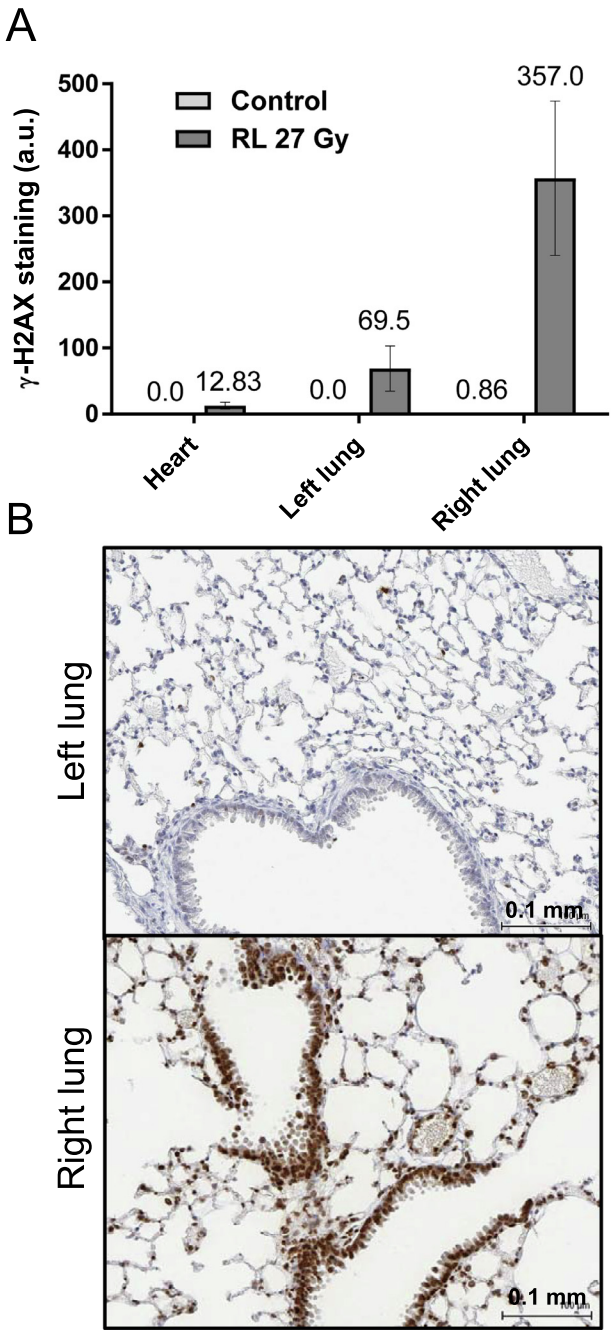

Fig. 2. (A) Quantification of γH2AX immunohistochemistry in heart, left or right lung 1 h after exposure of the right lung (RL) to 27 Gy or sham treatment in the controls. Mean ± SEM, $n = 6$ mice. (B) Microphotographs of representative γ-H2AX immunohistochemistry from the left and right lung of a mouse 1 h after right lung irradiation with 27 Gy.

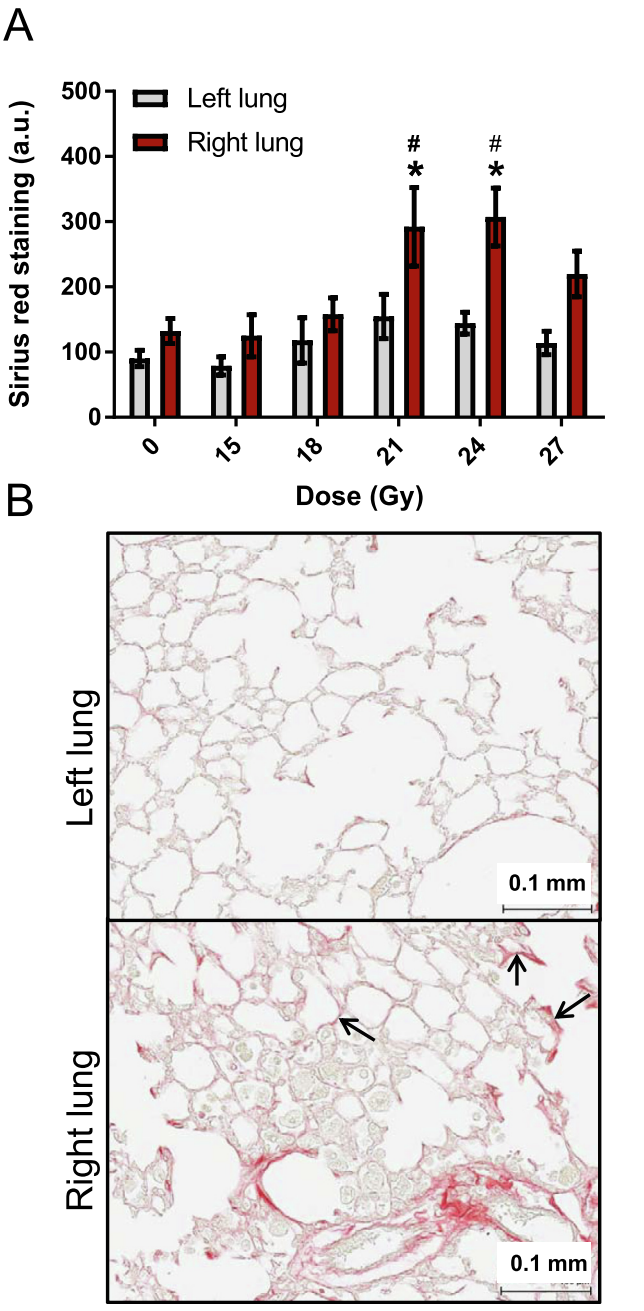

Fig. 3. (A) Quantification of Sirius red staining 40 weeks after sham-treatment or radiation of the right lung at indicated doses. Mean ± SEM, $n = 6$–10 mice; $^{*}p < 0.05$ vs. control, $^{\#}p < 0.05$ vs. left lung. (B) Microphotographs of representative Sirius staining from the left and the right lung of mouse that received 27 Gy on the right lung. Arrows indicate increased collagen deposition in the alveolar septa.

More than any histological parameter, this will ultimately determine the success of novel radiation-drug combination strategies. We therefore tested whether partial lung irradiation in this murine μIGRT lung fibrosis model impacts lung function and used a double-chamber plethysmography system to measure breathing rates in the mice. As shown in Fig. 4, we found a statistically significant increase in breathing rate ($p < 0.001$) in mice which received a radiation dose of 24 or 27 Gy to the right lung only. We conclude that our model shows the induction of lung function impairment by radiation, *i.e.* a "functionally-significant" fibrosis.

Radiation dose-dependent increase in μCBCT-determined lung density

X-ray and CT analyses are crucial to detect lung fibrosis in the clinic. Here, we assessed whether radiation-induced lung damage can be sensitively detected by μCBCT. μCBCT were performed at baseline and at multiple time points after radiation. Pleural effusions have been reported to occur after irradiation in a heart involvement dependent manner in some animal models. Pleural effusions, or signs thereof, were not detected on μCBCT images at any time point, nor by visual inspection after euthanasia or in the microscopy sections evaluation by the pathologist. Scans taken

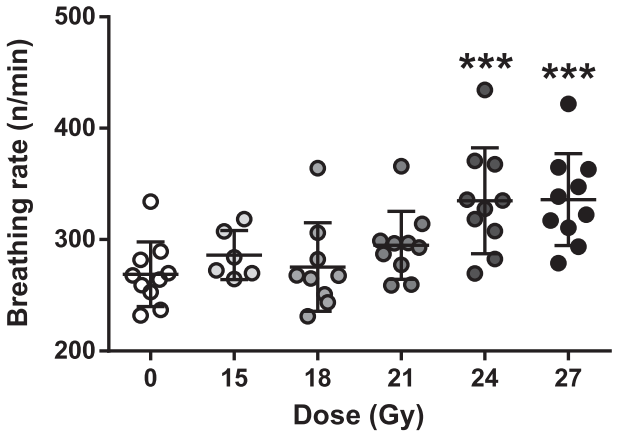

Fig. 4. Lung function measurement using double chamber plethysmography in mice 40 weeks after radiation. Data shown as mean breathing frequency ± SEM, $n = 6–10$ mice; $^{***}p < 0.001$ vs. control.

prior to euthanasia at 40 weeks post-irradiation were evaluated by delineating the large lung volumes while considering all planes ("whole-lung" in Sup-Fig. S6A). These preliminary data showed a marked increase in density in the radiated right lung of mice that were exposed to 21, 24 and 27 Gy ($p < 0.001$) warranting further μCBCT analyses.

To facilitate and improve lung density quantifications for large scale longitudinal studies, we approached the lung density assessment in a fully automated fashion ("fully automated" method). Due to their high density, large airways can cause substantial and radiation-independent variations in the data. The region of interest was placed in an area within the lung with a low presence of large airways and blood vessels to minimize the contribution of such lung components to the mean lung density values. These data were then compared and validated with density values as assessed by an alternative semi-automated data analysis procedure that was based on manual delineations ("2.5D" method) (Sup-Fig. S6B-C) and in which the density values were derived from a central slice in the coronal plane (Fig. 1D and E). We observe good concordance in the data and found high correlations with values above 0.95 (Sup-Fig. S6B-C). Importantly, we find a strong and significant radiation dose-dependent increase in density values (Fig. 5A–C for fully automated and Sup-Fig. S7 for semi-automated evaluations).

Changes in CT values are thought to reflect increased tissue densities due to fibrosis. We therefore compared the tissue density values as determined on the pathological tissue section material with the density values derived from μCBCT imaging. Fig. 5D demonstrates the association, both increasing greatly at 21 Gy. The μCBCT data are consistent with the histopathological assessments of fibrosis and show that μCBCT images and analyses reflect radiation induced lung damage well.

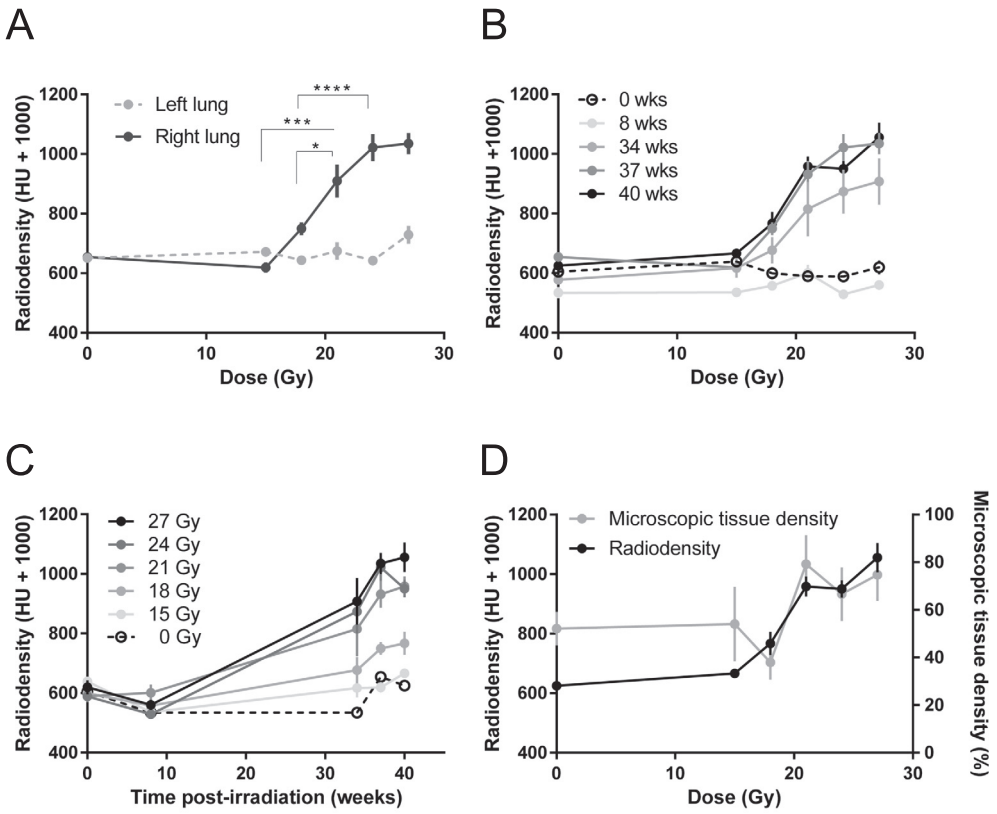

Fig. 5. (A) Radiodensity of the left and right lung assessed by μCBCT with the "fully automated" method as described in Materials and Methods and Sup-Fig. S1 and Sup-Methods, 37 weeks post-exposure. Mean ± SEM, $n = 4–5$ mice. Stars indicate p value levels determined by ANOVA: $^{*}<0.05$, $^{***}<0.001$, $^{****}<0.0001$. For simplicity, statistical test results of groups with >6 Gy dose differences are not shown. (B) Dose dependent development of right lung μCBCT-radiodensity over time. Mean ± SEM, $n = 4–5$ mice. (C) Time-dependent development of right lung radiodensity in the different radiation dose groups; mean ± SEM, $n = 4–5$ mice. (D) Comparison of lung density assessed by μCBCT (radiodensity left y-axis) and microscopic tissue density (right y-axis) at 40 weeks, as assessed by quantifying tissue per surface area on microscopic sections. Mean ± SEM, $n = 4–10$ mice.

Sensitive assessment of radiation induced lung damage

Given the observed strong radiation dose association, μCBCT scans could help to detect potential radiation response enhancements. Such non-invasive techniques also provide multiple test opportunities in longitudinal experimental designs to yield robust and sensitive measures of radiation damage. To further evaluate the dose- and time-dependent alterations in the lung in all mice, we determined lung densities at a range of time points. We found that radiodensity increased with time in the irradiated mice only and that this development depends on the radiation dose (Fig. 5-B-C, Sup-Fig. S7B-C). Even though there are signs of a plateau at high dose values, the data show that earlier assessments and/or lower radiation doses provide opportunities to sensitively detect lung damage changes in experimental regimes. Steep slopes (density increments per additional radiation dose) accompanied by a relative small variation in the data provided a good separation of individual dose groups (Fig. 5A and B). We find that 3 Gy or 6 Gy dose increments caused significant lung density changes in this model, thereby allowing the detection of relatively small but clinically relevant radiosensitization by experimental drug-radiation combination regimens.

Detection of lung damage aggravation by drug radiation combination treatment

Given the above revealed opportunity to sensitively detect small dose increments in this model, we next tested whether it would also allow the detection of additional lung damage caused by clinically applied radio-sensitizers. Cisplatin is an efficient and widely used radio-sensitizer that led to improved response rates after cisplatin-based chemoradiotherapy for lung cancer, however also provoked an increase in radiation induced toxicities.

We therefore tested whether our preclinical model would be able to depict changes in lung damage and performed an intervention study in which we treated mice with 21 Gy and cisplatin (3× 3 mg/kg b.w.) and then compared the μCBCT density changes of regular scans (every month) to radiated, solely cisplatin-treated or vehicle-treated controls (Fig. 6). μCBCT scan analyses were conducted as described above in a fully automated fashion. We find an accelerated onset of fibrosis in these mice, thereby showing that our model is able to reveal normal tissue (lung) radio-sensitization induced by drugs.

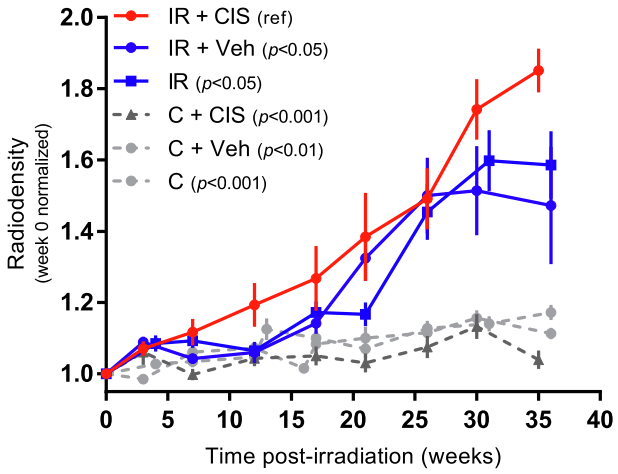

Fig. 6. Treatment induced μCBCT radiodensity changes after combined treatment of radiation and cisplatin. 21 Gy irradiated and cisplatin (3× 3 mg/kg) treated mice (IR + CIS, red dots) were compared to mice that were either irradiated (IR, blue triangles), received 21 Gy and *i.p.* injections of vehicle (IR + Veh, blue dots) or were sham-irradiated (0 Gy controls C) with or without cisplatin (CIS) or vehicle (Veh) in black and gray as indicated. Mean ± SEM, until 21 weeks n is 8–10 mice. Legend indicates significant differences in AUC when compared to the IR + CIS reference (ref).

Discussion

Here we set out to establish a relevant, robust and sensitive preclinical lung fibrosis model that enables the detection of potential risks in novel drug-radiation combinations. Using μIGRT and μCBCT we were able to minimize the involvement of the heart and sensitively detect lung damage aggravation. μCBCT density endpoints outperformed histochemical and lung function analyses in their sensitivity to detect radiation dose dependent changes.

Irradiated lung volumes strongly determine the odds of radiotherapy limiting lung fibrosis. In a similar study by Granton et al. that also shows the strength of μCBCT to assess lung damage, much smaller radiations fields were used [11]. Here, we purposely chose single fractions and large fields that maximize lung toxicity. This is to ensure the sensitive detection of any potential safety issues in novel drug-radiation combination strategies. Different doses were applied in small 3 Gy increments to assess the dose response in more detail. We found that lung μCBCT density changes, which reflect tissue density changes (Fig. 5D), develop over time. Initiation and extent of lung damage as determined by μCBCT is radiation-dose-dependent. Interestingly, both density measures (histochemistry and CBCT) reach a "saturation level" pointing to maximal achievable density values, a pattern which excludes technical (resolution) issues.

Radiation-induced lung fibrosis in C57Bl/6J mice has been well-studied [15,16]. Almost all of these studies applied old radiation techniques, often involving the whole or half of the thorax. Here we characterized the fibrotic radiation response and tested and compared several endpoints in our model that excludes critical organs. Aided by modern technologies, we were able to perform histopathological quantifications and found similar dose–response pattern as with the functional and imaging endpoints that we analyzed. Confirming radiation-induced fibrosis, collagen deposition increased in the right lung that had received 21, 24 or 27 Gy. The significant increase in breathing rates at higher doses further demonstrates the impact of right lung irradiation on lung function and excludes a large contribution from heart irradiation in the development of this pathology in mice in the earlier studies [18]. These lung function alterations also support the applicability of this model for preclinical safety testing. The application of modern animal lung function assessment equipment and technologies provided the required sensitivity to detect statistically significant changes. The lung damage-inducing radiation dose range observed in this study is comparable to earlier studies applying hemi-thorax irradiation or lower radiation volumes (recent μIGRT studies [11]). Considering the influence of critical organs, such as the heart or bone marrow, in the manifestation of lung damage or systemic drug toxicities, we attempted to minimize their role in our model, thus mimicking clinical practice. The considerable bone marrow radiation exposure of earlier models could be a strong confounding factor when assessing potential drug interactions. Here we reduced but did not fully exclude bone marrow irradiation. New models should consider exposures that are comparable to the clinic. The confounding effects from pleural effusion or from heart radiation were observed in other animal models [5,6,19,20]. It should be noted that these can vary in the different animal species and strains, as does also the link between radiation-induced pneumonitis and fibrosis. However, mice provide the advantage of being common test subjects in investigational studies that assess drug tolerance and efficacies. They also allow genetic manipulations to elaborate on mechanisms.

We found a marked dose- and time-dependent increase in the right lung density by μCBCT. Indeed, from all analyzed endpoints, μCBCT was found to be the most sensitive in detecting lung damage aggravation that were evoked by small dose increments. Others have also shown the strength of CT imaging in depicting lung damage in other models [21,22]. Here we showed that such analyses provide a sensitive measure of radiation-induced lung damage in mice. Fully automated μCBCT image analysis options facilitate repeated measurements in longitudinal large scale studies and thus strengthen the sensitivity to detect lung damage changes. This is crucial as we aim to detect potential dose intensifications by the combinations with drugs. In a recent study and despite promising early results, de Ruyscher et al. [23] were not able to demonstrate the pathologically assessed anti-fibrotic activity of nintedanib by μCT changes in their model [11]. Careful inspection of the data in the non-drug controls shows a considerable variation in the data that prevented the, in part linear, dose response relationship for most time points, suggesting their model did not provide sufficient sensitivity to depict such changes robustly [11,23]. The use of higher radiation doses and volumes resulted in a gradually increasing dose response curves at most time points in the here described model. Statistical significant differences in groups that differ by small dose increments (*e.g.:* 24 or 21 Gy *vs* 18 Gy) demonstrate that this experimental set-up improves consistency and sensitivity. Importantly, this translates to dose enhancement factors (DEF) as low as 1.2 or 1.4 that could be detected by such a model (illustrated in Sup-Fig. S8). To bring this into context: typical chemo-radiotherapy schedules apply radiosensitizers, for example cisplatin, that achieve DEFs of around 1.4 in tumor models. They however also cause significantly increased RILT in the clinic. Sensitive preclinical models that are able to depict such clinically relevant DEFs are needed [9,24]. We therefore combined the irradiation treatment with cisplatin and were able to show alterations in lung densities after such a combined drug/radiation treatment.

Novel drug/radiation combinations are mostly tested for efficient tumor radio-sensitization. Unfortunately, preclinical studies that alongside evaluate possible changes in radiation-induced toxicities are still much less numerous [25–27]. Although able to reveal some signals of increased toxicity in the case of the combination of radiation with the chemotherapeutic agent cisplatin, early studies lacked in part the sensitivity that novel technologies may be able to provide as shown here [28–34]. The urgent need for sensitive models to study novel drug/radiation combinations has led to high expectations toward the development of such models. While it is possible to adapt and optimize irradiation and imaging technologies to further approach the clinical situation, the use of small animals and their distinct biology limits the degree of similarity that can be achieved with such models. Lung toxicity is, for example, very difficult to evaluate utilizing current orthotopic lung tumor models. These often use immune-incompetent mice; or mice often succumb from their disease prior to any late lung toxicity development. Future genetic mouse tumor models may help to better assess novel treatment strategies. Yet, these factors are also likely to introduce a high degree of variation that in turn prevents the sensitive detection of any changes in radiation-induced toxicities. Here, we were able to increase the sensitivity to detect the exacerbation of an important radiation-induced lung pathology and therefore improved the suitability and significance of current radiation-induced lung toxicity mouse models. Strong signs of increased toxicities by certain drug radiation combinations, as revealed in such models, may call for careful and slow drug dose escalation designs in early Phase I clinical trials or may help to prioritize among different compounds of the same class. Hence, we propose the application of our and similarly sensitive and clinically relevant models in drug development pipelines that aim to improve lung radiotherapy.

To conclude, we established a preclinical partial radiation lung fibrosis model with heart exclusion and describe the dose dependent development of local fibrosis and overall lung function impairment under these conditions. Experimental set-up and μCBCT analyses permitted the sensitive and robust detection of lung damage, thus supporting the application in early drug-radiation combination developments for novel radiosensitizers or lung fibrosis mitigators.

Declaration of Competing Interest

The radiation oncology department of the Netherlands Cancer Institute licenses software for image registration to Precision X-ray Inc. The study was in part funded by license fees received from Elekta Oncology Ltd.

Acknowledgements

This study was in part supported by funds from the Dutch Cancer Society KWF (NKI 20104877). We highly appreciated Fiona Stewart's, Peter van Luijk's and Ghazaleh Ghobadi's advice on model design and CT lung pathology assessments. We would like to thank the people from the Preclinical Intervention Unit and Imaging Unit of the Mouse Clinic for Cancer and Ageing (MCCA) at the NKI for their help with the mouse studies and John Zavrakidis from the NKI biostatistics center for statistical support. We are grateful for funds received from AstraZeneca that supported research by CoV and DvB outside the scope of this study.

Appendix A. Supplementary data

Supplementary data to this article can be found online at https://doi.org/10.1016/j.radonc.2019.05.007.

References

[1] Auperin A, Le Pechoux C, Rolland E, et al. Meta-analysis of concomitant versus sequential radiochemotherapy in locally advanced non-small-cell lung cancer. J Clin Oncol 2010;28:2181–90.
[2] Furuta I. Ultrastructural and cellular damage to rat lung with x-rays - a search for target cell in lung tissue. Kobe J Med Sci 1975;21:1–15.
[3] Law MP, Hornsey S, Field SB. Collagen content of lungs of mice after X-ray irradiation. Radiat Res 1976;65:60–70.
[4] Ghobadi G, van der Veen S, Bartelds B, et al. Physiological interaction of heart and lung in thoracic irradiation. Int J Radiat Oncol Biol Phys 2012;84:e639–646.
[5] van Luijk P, Novakova-Jiresova A, Faber H, et al. Radiation damage to the heart enhances early radiation-induced lung function loss. Cancer Res 2005;65:6509–11.
[6] Jackson IL, Vujaskovic Z, Down JD. Revisiting strain-related differences in radiation sensitivity of the mouse lung: recognizing and avoiding the confounding effects of pleural effusions. Radiat Res 2010;173:10–20.
[7] Huang EX, Hope AJ, Lindsay PE, et al. Heart irradiation as a risk factor for radiation pneumonitis. Acta Oncol 2011;50:51–60.
[8] Clarkson R, Lindsay PE, Ansell S, et al. Characterization of image quality and image-guidance performance of a preclinical microirradiator. Med Phys 2011;38:845–56.
[9] Verhaegen F, Dubois L, Gianolini S, et al. ESTRO ACROP: Technology for precision small animal radiotherapy research: optimal use and challenges. Radiother Oncol 2018;126:471–8.
[10] Verhaegen F, Granton P, Tryggestad E. Small animal radiotherapy research platforms. Phys Med Biol 2011;56:R55–83.
[11] Granton PV, Dubois L, van Elmpt W, et al. A longitudinal evaluation of partial lung irradiation in mice by using a dedicated image-guided small animal irradiator. Int J Radiat Oncol Biol Phys 2014;90:696–704.
[12] van Hoof SJ, Granton PV, Verhaegen F. Development and validation of a treatment planning system for small animal radiotherapy: SmART-Plan. Radiother Oncol 2013;109:361–6.
[13] Down JD, Nicholas D, Steel GG. Lung damage after hemithoracic irradiation: dependence on mouse strain. Radiother Oncol 1986;6:43–50.

[14] Down JD, Steel GG. The expression of early and late damage after thoracic irradiation: a comparison between CBA and C57B1 mice. Radiat Res 1983;96:603–10.
[15] Jackson IL, Vujaskovic Z, Down JD. A further comparison of pathologies after thoracic irradiation among different mouse strains: finding the best preclinical model for evaluating therapies directed against radiation-induced lung damage. Radiat Res 2011;175:510–8.
[16] Sharplin J, Franko AJ. A quantitative histological study of strain-dependent differences in the effects of irradiation on mouse lung during the intermediate and late phases. Radiat Res 1989;119:15–31.
[17] Sharplin J, Franko AJ. A quantitative histological study of strain-dependent differences in the effects of irradiation on mouse lung during the early phase. Radiat Res 1989;119:1–14.
[18] Travis EL, Vojnovic B, Davies EE, Hirst DG. A plethysmographic method for measuring function in locally irradiated mouse lung. Br J Radiol 1979;52:67–74.
[19] van Luijk P, Novakova-Jiresova A, Faber H, et al. Relation between radiation-induced whole lung functional loss and regional structural changes in partial irradiated rat lung. Int J Radiat Oncol Biol Phys 2006;64:1495–502.
[20] van Luijk P, Faber H, Meertens H, et al. The impact of heart irradiation on dose-volume effects in the rat lung. Int J Radiat Oncol Biol Phys 2007;69:552–9.
[21] Schuster DP, Kovacs A, Garbow J, Piwnica-Worms D. Recent advances in imaging the lungs of intact small animals. Am J Respir Cell Mol Biol 2004;30:129–38.
[22] Nicholas D, Down JD. The assessment of early and late radiation injury to the mouse lung using X-ray computerised tomography. Radiother Oncol 1985;4:253–63.
[23] De Ruysscher D, Granton PV, Lieuwes NG, et al. Nintedanib reduces radiation-induced microscopic lung fibrosis but this cannot be monitored by CT imaging: A preclinical study with a high precision image-guided irradiator. Radiother Oncol 2017;124:482–7.
[24] Butterworth KT, Prise KM, Verhaegen F. Small animal image-guided radiotherapy: status, considerations and potential for translational impact. Br J Radiol 2015;88:20140634.
[25] Fokas E, Prevo R, Pollard JR, et al. Targeting ATR in vivo using the novel inhibitor VE-822 results in selective sensitization of pancreatic tumors to radiation. Cell Death Dis 2012;3:e441.
[26] Gani C, Coackley C, Kumareswaran R, et al. In vivo studies of the PARP inhibitor, AZD-2281, in combination with fractionated radiotherapy: An exploration of the therapeutic ratio. Radiother Oncol 2015;116:486–94.
[27] Lourenco LM, Jiang Y, Drobnitzky N, et al. PARP inhibition combined with thoracic irradiation exacerbates esophageal and skin toxicity in C57BL6 Mice. Int J Radiat Oncol Biol Phys 2018;100:767–75.
[28] Dewit L, Oussoren Y, Bartelink H, Thames HD. The effect of cis-diamminedichloroplatinum(II) on radiation damage in mouse rectum after fractionated irradiation. Radiother Oncol 1989;16:121–8.
[29] Kanazawa H, Rapacchietta D, Kallman RF. Schedule-dependent therapeutic gain from the combination of fractionated irradiation and cis-diamminedichloroplatinum (II) in C3H/Km mouse model systems. Cancer Res 1988;48:3158–64.
[30] Landuyt W, Ang KK, van der Schueren E. Combinations of single doses and fractionated treatments of cis-dichlorodiammineplatinum (II) and irradiation: effect on mouse lip mucosa. Br J Cancer 1986;54:579–86.
[31] Stewart F, Bohlken S, Begg A, Bartelink H. Renal damage in mice after treatment with cisplatinum alone or in combination with X-irradiation. Int J Radiat Oncol Biol Phys 1986;12:927–33.
[32] Stewart FA, Luts A, Oussoren Y, et al. Renal damage in mice after treatment with cisplatin and X-rays: comparison of fractionated and single-dose studies. NCI Monogr 1988:23–7.
[33] Veena K, Uma Devi P. Comparison of the toxic and radiosensitizing effects of five therapeutic drugs on the mouse jejunum. Strahlenther Onkol 1990;166:554–6.
[34] von der Maase H, Overgaard J, Vaeth M. Effect of cancer chemotherapeutic drugs on radiation-induced lung damage in mice. Radiother Oncol 1986;5:245–57.